Quantum Dots in Magnetic Fields: Phase Diagram and Broken Symmetry at the Maximum-Density-Droplet Edge

S. M. Reimann, M. Koskinen, and M. Manninen
Department of Physics, University of Jyväskylä, FIN-40351 Jyväskylä, Finland

B. R. Mottelson
NORDITA, Blegdamsvej 17, DK-2100 Copenhagen, Denmark
(Received 15 December 1998)

Quantum dots in magnetic fields are studied within the current spin-density-functional formalism avoiding any spatial symmetry restrictions of the solutions. We find that the maximum-density droplet reconstructs into states with broken internal symmetry: The Chamon-Wen edge coexists with a modulation of the charge density along the edge. The phase boundaries between the polarization transition, the maximum-density droplet, and its reconstruction are in agreement with recent experimental results.

PACS numbers: 73.20.Dx, 73.40.Hm, 85.30.Vw

Quantum dots are small electron islands made by laterally confining the two-dimensional electron gas in a semiconductor heterostructure. Such nanosized systems attracted much interest since the techniques in their fabrication developed far beyond mesoscopic dimensions [1]. Vertical quantum dots can nowadays be made so small that they show atomlike behavior [2]: shell structure and Hund's rules determine the electronic properties.

Much experimental effort focused on systematically mapping the magnetic field dependence of the chemical potential obtained from single-electron capacitance spectroscopy [3]. As a bias is applied to the gates, single electrons tunnel into the quantum dot when its chemical potential $\mu(N, B)$ (which depends on the number of confined electrons N and the magnetic field strength B) equals the Fermi energy in one gate electrode. First experiments along these lines were performed by Ashoori *et al.* [3] and later Klein *et al.* [4]. Recently, Oosterkamp *et al.* [5] systematically extended the measurements to stronger fields B and larger sizes N. Cusps and steps in $\mu(N, B)$ were found to clearly separate different ranges of magnetic fields. From a comparison to results of exact diagonalization studies [6] these patterns were identified with phase transitions in the droplet: they occur at magnetic fields for which the ground-state charge distribution of the dot changes, defining sharp phase boundaries. The points at which a complete polarization of the electrons occurs mark the beginning of the so-called maximum density droplet (MDD) phase. This new state suggested by McDonald, Yang, and Johnson [7] is a homogeneous droplet in which the density is approximately constant at the maximum value $\rho_0 = (2\pi l_B^2)^{-1}$ that can be reached in the lowest Landau level. ($\ell_B = \sqrt{\hbar/eB}$ is the magnetic length). In the spin-polarized MDD the electrons occupy adjacent orbitals with consecutive angular momentum. This compact occupation of states maximizes the electron density. The stability of the MDD is determined by a competition between the kinetic and external confinement contributions to the total energy, and the Coulomb repulsion of the electrons. The former would favor the MDD structure up to infinite fields: with increasing B, the droplet would decrease in radius such that close to the dot center it could maintain a density corresponding to filling factor one in the bulk limit [8]. This, however, is inhibited by Coulomb repulsion: At a sharply defined transition point, the charge density distribution of the droplet reconstructs [7,9]. Chamon and Wen [9] found from Hartree-Fock calculations that at the edge of a quantum Hall liquid with bulk filling factor one, a stripe or ring of electron density breaks off from the homogeneous bulk or the MDD phase.

In this Letter, we show that the so-called Chamon-Wen edge actually is a ring of nearly localized electrons surrounding the MDD (see Fig. 3 below). Moreover, we find that the calculated phase boundaries are in good qualitative agreement with recent experimental results [5].

As exact diagonalization techniques [6] are limited to small particle numbers, mean-field methods are needed to simplify the complicated many-body problem. We apply the so-called current spin density functional theory (CSDFT) [10] including gauge fields in the energy functional. In contrast to the HF calculations by Chamon and Wen [9] or recent applications of CSDFT [11–13] we avoid any spatial symmetry restrictions of the mean-field solution.

As a basic model for a quantum dot one usually considers N interacting electrons of effective mass m^* confined in a two-dimensional harmonic trap. A homogeneous magnetic field $\mathbf{B} = B\mathbf{e}_z$ is applied perpendicular to the x-y plane in which the electrons are confined by the external potential $V = m^*\omega^2 r^2/2$. In a symmetric gauge, the external vector potential acting on the electrons is $\mathbf{A} = B/2(-y, x)$. For the details of CSDFT we refer to the work of Vignale and Rasolt [10] and recall here only the most important steps. The self-consistent Kohn-Sham

 0031-9007/99/83(16)/3270(4)$15.00

type equations in CSDFT read

$$\left[\frac{\mathbf{p}^2}{2m^*} + \frac{e}{2m^*}(\mathbf{p}\cdot\mathcal{A} + \mathcal{A}\cdot\mathbf{p}) + \mathcal{V}_\delta\right]\Psi_{i\delta} = \varepsilon_{i\delta}\Psi_{i\delta}\,.$$

(We have dropped the arguments $\mathbf{r}$ for simplicity). The index i labels the eigenstates with spin $\delta = (\uparrow,\downarrow)$. We defined effective vector and scalar potentials $\mathcal{A} := \mathbf{A} + \mathbf{A}_{\rm xc}$ and $\mathcal{V}_\delta := (e^2/2m^*)A^2 + V_\delta + V_H + V_{{\rm xc}\delta}$. Here, V_H is the ordinary Hartree potential and $V_\delta = V + (-)g^*\mu_B B/2$ is the external potential, including the Zeeman energy. [$\mu_B = e\hbar/(2m_e)$ is the Bohr magneton]. The exchange-correlation vector and scalar potentials are

$$e\mathbf{A}_{\rm xc} = \frac{1}{\rho}\left\{\frac{\partial}{\partial y}\frac{\partial[\rho e_{\rm xc}(\rho_\delta,\gamma)]}{\partial\gamma}, -\frac{\partial}{\partial x}\frac{\partial[\rho e_{\rm xc}(\rho_\delta,\gamma)]}{\partial\gamma}\right\}$$

and

$$V_{{\rm xc}\delta} = \frac{\partial[\rho e_{\rm xc}(\rho_\delta,\gamma)]}{\partial\rho_\delta} - \frac{e}{\rho}\,\mathbf{j}_p\cdot\mathbf{A}_{\rm xc}\,,$$

where ρ is the particle density $\rho = \rho_\uparrow + \rho_\downarrow$ with $\rho_\delta = \sum_i |\Psi_{i\delta}|^2$. The paramagnetic current density is given by $\mathbf{j}_p = -i\hbar/(2m^*)\sum_{i\delta}[\Psi^*_{i\delta}\nabla\Psi_{i\delta} - \Psi_{i\delta}\nabla\Psi^*_{i\delta}]$ and the real current density equals $\mathbf{j} = \mathbf{j}_p + (e/m^*)\mathbf{A}\rho$. In essence and as applied in CSDFT, the exchange-correlation energy depends on the so-called vorticity $\gamma = \nabla\times(\mathbf{j}_p/\rho)|_z$ of the wave function. In the bulk the total current density must be zero, and thus $\gamma = -eB/m^*$. It is this relation that allows us to use the interpolation formulas for the exchange energy per particle $e_{\rm xc}$ for the homogeneous bulk in CSDFT by replacing $B \to (m^*/e)\,|\gamma|$. Making use of the local spin density approximation (LSDA), the exchange energy per particle $e_{\rm xc}$ is parametrized in terms of the local particle density ρ, the spin polarization $\xi = (\rho_\uparrow - \rho_\downarrow)/\rho$, and the filling factor $\nu = 2\pi\hbar\rho/m^*|\gamma|$. We used the expression $e_{\rm xc}(\rho,\xi,\nu) = e^\infty_{\rm xc}(\rho)e^{-f(\nu)} + e^{\rm TC}_{\rm xc}(\rho,\xi)\,(1 - e^{-f(\nu)})$, where $f(\nu) = 1.5\nu + 7\nu^4$. This form interpolates between the infinite magnetic field limit $e^\infty_{\rm xc}(\rho) = -0.782\sqrt{2\pi\rho}e^2/4\pi\epsilon_0\epsilon$ and zero field limit $e^{\rm TC}_{\rm xc}(\rho,\xi)$, for which we use the Tanatar-Ceperly [14] functional and generalize it to intermediate polarizations [15]. For $\nu < 0.9$, the interpolation in $e_{\rm xc}(\rho,\xi,\nu)$ follows closely the results of Fano and Ortolani [16] for polarized electrons in the lowest Landau level, and saturates quickly to the zero field result for $\nu > 1$.

The LSDA has been shown to describe very accurately addition spectra [3–5] in weak or zero fields [13,17]. Here we concentrate on the polarization transition and beyond. We use a plane wave basis to solve the single-particle Kohn-Sham equations self-consistently. The practical computational techniques which we found necessary to obtain converged solutions of the CSDFT mean field equations are described in Ref. [18]. For the material parameters we choose the typical GaAs values for the effective mass $m^* = 0.067m_e$, the dielectric constant $\varepsilon = 12.4$, and the reduced Landé g-factor $g^* = 0.44$. (This yields an effective Bohr radius of $a^*_B = 9.79$ nm.) The strength of the external confinement is set to $\hbar\omega = 4.192N^{-1/4}$ meV. For different N, this convention keeps the average electron density in the droplet approximately constant, in this case roughly corresponding to a (two-dimensional) Wigner-Seitz radius $r_s = 2a^*_B$.

As a first example, we study $N = 20$ electrons confined in the above specified GaAs dot. At a field of about 2.3 T, only one minority spin is left in the dot center. The droplet becomes completely polarized for fields larger than about 2.4 T. Shortly after the polarization point the MDD is formed. Its density profile has perfect azimuthal symmetry and is nearly constant inside the droplet corresponding to filling factor one in the bulk: all electrons are in the lowest Landau level and all single-particle states are occupied by one spin down electron with successive angular momenta $m = 0, 1, \ldots, N-1$ [19]. The total orbital angular momentum then is $M = \frac{1}{2}N(N-1)$, which yields $M = 160$. As in the inner regions of the MDD the filling factor equals 1, the density rises with increasing magnetic field, and the whole droplet decreases in radius. For $N = 20$ the MDD is stable for fields up to $B \lesssim 2.9$ T, where the reconstruction of the charge density distribution begins. The density distribution of the MDD at $B = 2.9$ T is shown in the upper panel of Fig. 1.

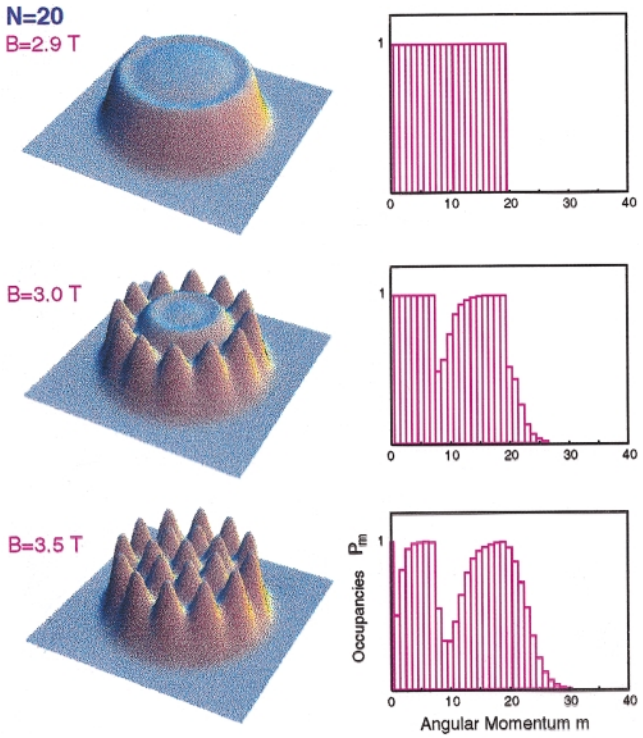

FIG. 1 (color). Self-consistent densities for a 20-electron GaAs quantum dot shortly before edge reconstruction at $B = 2.9$ T (top), forming the broken-symmetry Chamon-Wen edge at 3.0 T (middle) and being fully reconstructed at 3.5 T (bottom). Right: Angular momentum occupancies P_m as defined in the text.

We can gain information about the angular momentum occupancy in the droplet by projecting the Kohn-Sham single-particle wave functions $|\Psi_{i\downarrow}\rangle$ on Fock-Darwin [20] states $|nm\rangle$ with radial quantum number n and good angular momentum m. Summing over all occupied states $i \leq N$, we obtain the total angular momentum occupancy $P_m = \sum_{i,n} |\langle nm \,|\, \Psi_{i\downarrow}\rangle|^2$ with $i \leq N$. (In strong fields, only $n = 0$ states give a significant contribution.) The values of P_m are plotted with bars for each m value in the right column of Fig. 1. As expected, for the MDD all angular momenta up to $N - 1$ have occupancy one.

Increasing the magnetic field effectively compresses the electron states, such that states with constant m decrease in radius. Consequently, the density of the MDD would continuously increase with B. This, however, is inhibited by the Coulomb interaction. The droplet thus redistributes [9] its density over the dot area, taking advantage of moving electrons from lower to higher angular momentum states and leaving some partly unoccupied states for $m < N - 1$. Thus, $M > N(N - 1)/2$ and the Chamon-Wen edge is formed [9]. The corresponding density and angular momenta at $B = 3.0$ T are shown in the middle panel of Fig. 1. After reconstruction, the *MDD has thrown out a ring of separate lumps of charge density*, with each lump containing one electron and having a radius somewhat larger than the magnetic length ℓ_B. This Chamon-Wen edge with broken rotational symmetry is located at a distance of $\sim 2\ell_B$ from the inner part of the droplet, which continues to form a (smaller) MDD with filling factor 1 in the dot center. With the reconstruction of the droplet, fractions of angular momenta between $m = 8$ and $m = 14$ are moved to values above $m = 19$. The total angular momentum now is raised to $M = 205.13$. (Note that for the *internally* broken symmetry of the mean-field solution, the total angular momentum can take fractional values.)

The total current $\mathbf{j}(x, y)$ is plotted as a vector diagram in Fig. 2. It shows vortices which are located around the density maxima along the edge.

For still higher fields, rotational symmetry is also broken for the inner parts of the droplet (see lowest panel in Fig. 1). The reconstructed density forms a *sequence of rings*, each consisting of well-separated maxima in the electron density. Correspondingly, inside the droplet the real current $\mathbf{j}(x, y)$ now forms vortices (see right panel of Fig. 2) centered at the separate density maxima along the rings. The localization of all electrons is associated with opening a large gap at the Fermi level. This had not been the case if only electrons along the edge were localized, as the inner part of the droplet then still was in the MDD phase. In the high-field limit, the "bumpy" electron density is consistent with the numerical results of HF calculations by Müller and Koonin [21]. Performing exact calculations for $N \leq 6$, Maksym [22] found localized states using a rotating frame.

The broken symmetry of the Chamon-Wen edge is not limited to small dots. Figure 3 shows the density and

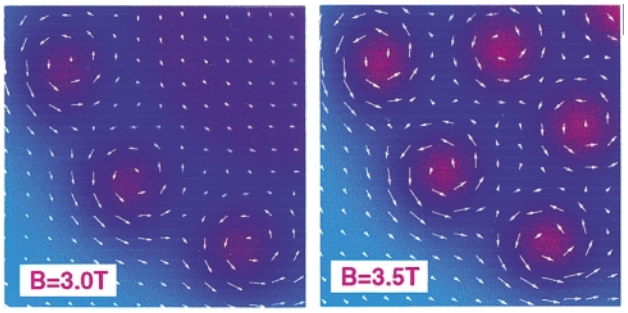

FIG. 2 (color). Real particle current $\mathbf{j}(\mathbf{r})$ for $N = 20$ at $B = 3.0$ T (left) and $B = 3.5$ T (right), shown in the lower left quadrant of the charge density. The maximum currents are about 0.028 $(\text{nm ps})^{-2}$ (at 3.0 T) and 0.035 $(\text{nm ps})^{-2}$ (at 3.5 T). The shaded background indicates the charge density distribution: areas colored in magenta correspond to the regions with largest charge density.

angular momentum distribution of a dot with $N = 42$ electrons. Again the edge consists of nearly localized electrons. The inner MDD at filling factor 1 is very stable, with integer occupancy of angular momentum. By analyzing the Kohn-Sham single-particle orbitals we noticed that they fall into two discrete subsets, one forming the MDD and the other forming the broken-symmetry Chamon-Wen edge. This opens up a possibility for collective excitations localized at the edge.

We finally study the formation of the MDD and its reconstruction systematically as a function of the electron number. The resulting phase diagram is shown in Fig. 4. We find three phase boundaries: the polarization transition with the subsequent formation of the MDD, the broken-symmetry Chamon-Wen edge phase, and finally the localization phase [21] where the MDD completely disappears. The range of magnetic fields where the MDD is a stable ground state becomes much more narrow with increasing N, as it has been noted in Refs. [7,9,23]. The phase boundaries are in good agreement with recent experiments by Oosterkamp *et al.* [5]. (The fact that we find the transitions between different phases at smaller fields is due to a different electron density [24]). The experimental results also show systematic changes in the chemical potential after the first appearance of the Chamon-Wen edge. This might be related to the formation of rings and the stepwise disappearance of the MDD, which has a similar dependence of the number of electrons and the magnetic field.

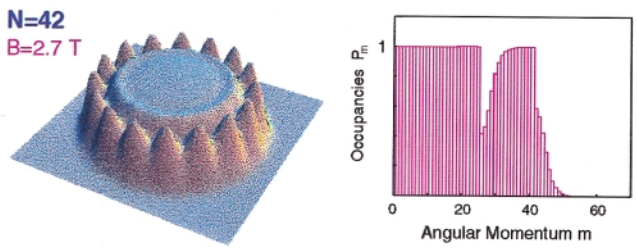

FIG. 3 (color). As Fig. 1, but for $N = 42$ electrons and at a magnetic field $B = 2.7$ T.

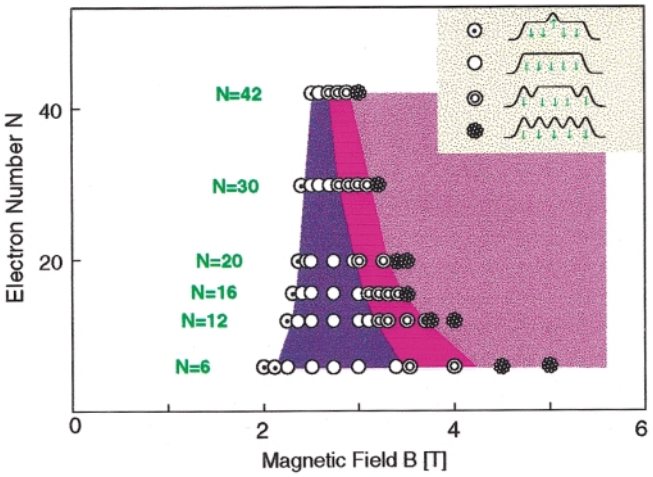

FIG. 4 (color). Different phases for a quantum dot with $N = 6$, 12, 16, 20, 30 and $N = 42$ electrons at a density roughly corresponding to $r_s = 2a_B^*$. The colored areas indicate regions of magnetic fields where different phases (polarization, MDD, reconstruction, and beyond) occur: The purple region indicates the MDD phase, while the magenta region corresponds to the Chamon-Wen edge regime. In the pink region localization extends over the whole droplet.

We have exclusively investigated the reconstruction in the regime where the droplet was completely polarized and refer to [25,26] for a discussion about the existence of spin textures along the edges. Performing fully unrestricted Hartree-Fock calculations, Karlhede and Lejnell [25] as well as Franco and Brey [26] found charge density wavelike modulations along the reconstructed edge of a Hall bar. These results are similar to our finding of the broken-symmetry edge in *finite* droplets.

In conclusion, we found that the maximum density droplet reconstructs into *Chamon-Wen edge states with broken rotational symmetry* in the internal coordinates. For larger fields reconstruction continues by sequential formation of rings up to an overall bumpy ground state density. The transitions with increasing B define different phases of the electron liquid inside the droplet. We showed a phase diagram which displayed a systematic separation between different phases of reconstruction both as a function of dot size and magnetic field. The trends for the shape of the phase boundaries between polarization transition, MDD, broken symmetry edge reconstruction, and finally localized states [21] are rather clear and agree [24] with the phase diagram recently measured by Oosterkamp *et al.* [5].

We acknowledge discussions with D. G. Austing and S. Viefers. This work was supported by the Academy of Finland, the Studienstiftung des deutschen Volkes and the TMR programme of the European Community under Contract No. ERBFMBICT972405.

[1] L. P. Kouwenhoven *et al.*, in *Proceedings of the Advanced Study Institute on Mesoscopic Electron Transport, 1997*, edited by L. L. Sohn, L. P. Kouwenhoven, and G. Schön.
[2] S. Tarucha, D. G. Austing, T. Honda, R. J. van der Hage, and L. P. Kouwenhoven, Phys. Rev. Lett. **77**, 3613 (1996).
[3] R. Ashoori, H. L. Störmer, J. S. Weiner, L. N. Pfeiffer, K. W. Baldwin, and K. W. West, Phys. Rev. Lett. **71**, 613 (1993); R. Ashoori, Nature (London) **379**, 413 (1996).
[4] O. Klein, C. de Chamon, D. Tang, D. M. Abusch-Magder, U. Meirav, X.-G. Wen, M. A. Kastner, and S. J. Wind, Phys. Rev. Lett. **74**, 785 (1995).
[5] T. H. Oosterkamp, J. W. Jansen, L. P. Kouwenhoven, D. G. Austing, T. Honda, and S. Tarucha, cond-mat/9810159 [Phys. Rev. Lett. (to be published)].
[6] See, for example, A. H. MacDonald and M. D. Johnson, Phys. Rev. Lett. **70**, 3107 (1993); P. Hawrylak, Phys. Rev. Lett. **71**, 3347 (1993); J. J. Palacios *et al.*, Phys. Rev. B **50**, 5760 (1994); to mention only a few.
[7] A. H. McDonald, S. R. Eric Yang, and M. D. Jonson, Aust. J. Phys. **46**, 345 (1993).
[8] The bulk filling factor reflects the Landau level occupation close to the dot center in the limit of strong fields (see Palacios *et al.* in Ref. [6]).
[9] C. de Chamon and X. G. Wen, Phys. Rev. **49**, 8227 (1994).
[10] G. Vignale and M. Rasolt, Phys. Rev. B **37**, 10 685 (1988).
[11] M. I. Lubin, O. Heinonen, and M. D. Johnson, Phys. Rev. B **56**, 10 373 (1997).
[12] M. Pi, M. Barranco, A. Emperador, E. Lipparini, and Ll. Serra, Phys. Rev. B **57**, 14 783 (1998).
[13] O. Steffens, U. Rössler, and M. Suhrke, Europhys. Lett. **42**, 529 (1998).
[14] B. Tanatar and D. M. Ceperley, Phys. Rev. B **39**, 5005 (1989).
[15] M. Koskinen, M. Manninen, and S. M. Reimann, Phys. Rev. Lett. **79**, 1389 (1997).
[16] G. Fano and F. Ortolani, Phys. Rev. B **37**, 8179 (1988).
[17] S. M. Reimann, M. Koskinen, M. Manninen, D. G. Austing, and S. Tarucha, Eur. J. Phys. (to be published).
[18] M. Koskinen, J. Kolehmainen, S. M. Reimann, J. Toivanen, and M. Manninen, Eur. J. Phys. D (to be published).
[19] Note that we omit the negative sign of angular momentum eigenvalues here and in the following.
[20] V. Fock, Z. Phys. **47**, 446 (1928); C. G. Darwin, Proc. Cambridge Philos. Soc. **27**, 86 (1931).
[21] H.-M. Müller and S. E. Koonin, Phys. Rev. B **54**, 14 532 (1996).
[22] P. A. Maksym, Europhys. Lett. **31**, 405 (1995); Phys. Rev. B **53**, 10 871 (1996).
[23] M. Ferconi and G. Vignale, Phys. Rev. B **56**, 12 108 (1997).
[24] For the experimental data the average density was estimated to correspond to a density parameter of about $r_s = 1.3a_B^*$ [D. G. Austing (private communication)].
[25] A. Karlhede, S. A. Kivelson, K. Lejnell, and S. L. Sondhi, Phys. Rev. Lett. **77**, 2061 (1996); A. Karlhede and K. Lejnell, cond-mat/9709339.
[26] M. Franco and L. Brey, Phys. Rev. B **56**, 10 383 (1997).